Clay Minerals, (2013) **48**, 529–541

Experimental and theoretical evidence of zinc structurally bound in vermiculite from naturally metal-enriched soils

J. C. FERNÁNDEZ-CALIANI[1,2,*], V. TIMÓN[3], M. B. RIVERA[1], I. GIRÁLDEZ[4] AND R. PÉREZ-LÓPEZ[1]

[1] *Department of Geology, University of Huelva, 21071-Huelva, Spain,* [2] *Center for Research in Sustainable Chemistry (CIQSO), University of Huelva, 21071-Huelva, Spain,* [3] *Andalusian Institute of Earth Sciences, Spanish Research Council-University of Granada, 18100-Armilla, Granada, Spain, and* [4] *Department of Chemistry and Materials Sciences, University of Huelva, 21071-Huelva, Spain*

(*Received 14 January 2013; revised 16 April 2013; Editor: Juan Cornejo*)

ABSTRACT: This paper provides evidence of appreciable amounts of Zn (up to 0.52 a.p.f.u.) residing in the crystal structure of trioctahedral vermiculite; the results were obtained by a combination of experimental methods (X-ray diffraction, energy dispersive X-ray spectrometry, electron microprobe analysis and selective chemical extractions) and theoretical studies based on density functional theory (DFT). Vermiculite occurs in size fractions ranging from 10 to 40 μm of near-neutral soils naturally enriched in Zn (up to 8110 mg kg^{-1}) due to the weathering of carbonate-hosted Zn-Pb deposits in SW Spain. Zinc was partitioned among the various pedogenic phases during soil formation, but the larger part (>80%) was concentrated in the residual silicate fraction. The soil exchangeable Zn pool was found to be virtually negligible. The DFT calculations support the hypothesis that the role of vermiculite is an effective sink for geogenic Zn; this is consistent, in terms of energetic stability, with the assumption that most Zn is structurally bound in octahedral sheets rather than in the interlayer exchange sites. The findings conclusively indicate that the potential mobility of Zn should remain low under the present soil conditions.

KEYWORDS: zinc, vermiculite, soil, geogenic enrichment, metal partitioning, selective chemical extractions, density functional theory.

Metals released from weathering of sulfide-bearing rocks and mineralized veins may be accumulated in near-surface environments through different retention mechanisms (e.g. Evans, 1989), providing exceptionally high metal concentrations of geogenic origin. It is recognized that layered minerals are efficient sinks for metals in soils and sediments. Studying the uptake mechanisms of metals on clays in pristine soils may provide valuable information about the long-term fate of such potentially hazardous elements, and also support the optimization of remediation strategies for contaminated soils (Jacquat *et al.*, 2009a).

Recent spectroscopic studies on the speciation of metals in pristine and contaminated soils have shown that the formation of layered minerals, such as hydroxides, layered double hydroxides (LDH) and phyllosilicates may be a relevant sequestration mechanism (Manceau *et al.*, 2000, 2004; Scheinost *et al.*, 2002; Juillot *et al.*, 2003; Jacquat *et al.*, 2008, 2009a,b; Voegelin *et al.*, 2011). In soils derived from weathered Zn-sulfide ore deposits, a variety of Zn-rich phyllosilicates have been

* E-mail: caliani@uhu.es
DOI: 10.1180/claymin.2013.048.3.09

identified, including Zn-kerolite, fraipontite (Zn-serpentine), sauconite (Zn-smectite), baileychlore (Zn-chlorite), and hydroxy-interlayered minerals (vermiculites and smectites) (Jacquat, 2008, and references therein).

In phyllosilicates, Zn may be incorporated in, or sorbed on, the octahedral sheet or a hydroxy-Al sheet in the interlayer region (Manceau *et al.*, 2004). Specific sorption of Zn in the interlayer of hydroxy-interlayered vermiculite (HIV) is an important Zn uptake mechanism in acid soils exposed to frequent wetting and drying cycles and with low organic matter content (Rich, 1968; Yin *et al.*, 2013) that are too acidic to retain Zn by formation of inner-sphere sorption complexes or layered double hydroxides (Scheinost *et al.*, 2002). However, HIV does not allow for the accumulation of high levels of Zn in response to continued Zn input into soils due to its limited sorption capacity (Jacquat *et al.* 2008, 2009b,c).

In this paper, we have investigated vermiculitic soils with geogenically elevated metal contents in order to assess the role of vermiculite in Zn sequestration during soil development, and its environmental implications for long-term metal retention. The key objectives were: (1) to ascertain the geochemical partitioning and reactivity of Zn in soil; and (2) to elucidate the dominant residence site for Zn within the vermiculite structure.

MATERIALS AND METHODS

Sampling and sample pre-treatment

The samples studied came from unpolluted chestnut grove soils located in the central part of the Aracena and Picos de Aroche Natural Park, in Huelva province (SW Spain). In this area, the soils derived from a Lower Cambrian sequence of metavolcanic and carbonate rocks, host stratabound Pb-Zn-Ag deposits with sphalerite, galena and pyrite being the dominant ore minerals (Fernández-Caliani *et al.*, 1989; Arribas *et al.*, 1990). As a result of intensive chemical weathering of the sulfide-bearing parent rocks, the soils have been naturally enriched in Zn and other potentially toxic elements (Galán *et al.*, 2008).

Five profiles were selected to represent the geogenically Zn-rich soils in the area, classified as Eutric Cambisols according to Junta de Andalucía (1989). Their topsoil samples (0−20 cm depth) were collected using an Edelman auger and immediately transferred to plastic bags. The soil samples were air-dried at room temperature, gently crushed to break aggregates, homogenised, and then passed through a 2 mm stainless-steel sieve for determining soil properties (texture, pH, Eh and electrical conductivity) and for chemical extractions. Aliquots of the sieved material were ground in an agate mortar to recover the <63 μm grain-size powder for mineralogical and chemical analyses. The clay fraction (<2 μm) was extracted from the whole sample after dispersion in deionised water and centrifugation. The soil samples were also mounted in epoxy, polished and carbon-coated for electron microscope examination and electron probe microanalysis.

Chemical extraction methods

Geochemical partitioning and reactivity of Zn in soil materials were investigated using single and sequential extractions. Two commonly used single-reagent extraction tests with 1 M $MgCl_2$ and with 1 M NH_4OAc were applied to assess the exchangeable and weakly adsorbed fraction of Zn (Ure, 1996). An aliquot of each air-dry soil sample was subjected to chemical extraction by shaking for 1 h with both neutral salt solutions at a soil:solution ratio of 1:10 (w/v). The single extraction procedure was repeated three times for each soil sample.

The sequential extraction scheme proposed by the European Standards, Measurements and Testing (SM&T) Program, formerly the Community Bureau of Reference (BCR), was applied for Zn partitioning among three operationally-defined geochemical fractions (acid soluble/exchangeable, reducible and oxidizable). Experimental details are provided in Quevauviller *et al.* (1994). The conventional BCR method was modified at each stage, applying ultrasonic energy with a Sonopuls ultrasonic homogenizer fitted with a HF generator 2200, in order to accelerate the extraction process (Pérez-Cid *et al.*, 1998). The selective extractions were conducted in stoppered polyethylene centrifuge tubes at room temperature. Between each successive extraction, separation was achieved by centrifugation at 5000 rpm for 10 min. The supernatant was then removed with a Pasteur pipette and stored at 4ºC until analysis; the residue was washed with deionised water.

The Zn concentration in the residual fraction (i.e. the metal content structurally bound in silicates) was determined after multi-acid digestion of the

residue with a mixture of $HClO_4$-HNO_3-HCl-HF that ensured dissolution of the entire sample. All digestions and sequential extractions steps were conducted in triplicate. The chemical extraction agents used in the sequential extraction procedure are summarized in Table 1. All the reagents were of analytical grade Suprapur quality, and ultrapure water obtained from a Milli-Q purifier system was used throughout the work.

Apparatus and instrumental conditions

Textural information was obtained by laser diffraction particle-size analysis, using a Malvern Mastersizer 2000 instrument. Soil reaction (pH), redox potential (Eh) and electrical conductivity (EC) were potentiometrically measured in the supernatant of a 1:2.5 (w/v) soil:deionized water suspension, after shaking for 15 min followed by a 30 min equilibration period.

Mineralogical analysis was carried out by powder X-ray diffraction (XRD) on a Bruker AXS D8-Advance diffractometer using Ni-filtered Cu-$K\alpha$ radiation at 40 kV and 30 mA. Randomly oriented powders were scanned from 3 to 65º 2θ with a step size of 0.02º and a counting time of 0.6 s per step. Oriented clay films were obtained from sedimentation of soil suspension onto glass slides and then analysed in the air-dried state (natural and Mg-exchanged) after ethylene glycol solvation (vapour at 60ºC for 48 h) and after heating at 300ºC and at 550ºC for 2 h. The oriented aggregates were scanned from 1 to 30º 2θ using a step size of 0.02º and a counting time of 1.2 s per step. The relative mineral abundance was semi-quantitatively estimated on randomly oriented powders (bulk mineralogy) and oriented aggregates (clay mineralogy) by empirical factors weighting the integrated peak areas of distinctive reflections (Schultz, 1964; Biscaye, 1965).

The soil samples were examined by scanning electron microscopy (SEM) on carbon-coated loose powder mounts, using a JEOL JSM-5410 instrument operated at 20 kV, and equipped with an energy dispersive X-ray (EDS) analytical system (Oxford Link ISIS).

Chemical analysis of major elements in bulk samples was done by X-ray fluorescence spectrometry (XRF) with a Bruker AXS S4 Pioneer apparatus, using fused glass disks prepared with 1:10 proportion of sample:flux. Calibration curves were based on certified standard samples.

Electron probe microanalysis (EPMA) of selected vermiculite crystals was performed on a JEOL JXA-8200 SuperProbe equipped with four wavelength dispersive X-ray spectrometers (WDS), an EDS spectrometer and back-scattered (BSE) and secondary electron (SE) detectors. Quantitative chemical analysis was carried out by WDS using an accelerating voltage of 15 kV, a beam current of 20 nA, and a beam diameter of up to 5 μm. A combination of well-characterized minerals and synthetic materials was used as standard for calibration, and the conventional ZAF correction procedure was applied to the data.

The total concentration of Zn in bulk soil samples was determined by inductively coupled plasma-optical emission spectrometry (ICP-OES) at the Activation Laboratories Ltd. (Canada), which is accredited to the ISO/IEC 17025 Quality System. The quality control method included the use of a reagent blank, certified reference materials and replicates. The average accuracy of the analytical data was ±5%.

Concentrations of Zn extracted with $MgCl_2$ and NH_4OAc were measured, after centrifugation at

TABLE 1. Selective sequential extraction procedure (formerly BCR scheme, modified by Perez-Cid *et al.*, 1998), chemical extractants and conditions used in this study.

Fraction	Operational definition	Reagents and conditions	Sonication time
F1	Acid-soluble/exchangeable fraction	20 mL 0.11 M HOAc	7 min
F2	Reducible fraction	20 mL 0.1 M $NH_2OH{\cdot}HCl$ (pH 2)	7 min
F3	Oxidizable fraction	10 mL H_2O_2 30% (w/v) (evaporated to 1–2 mL) 25 mL 1 M NH_4OAc	2 min 6 min
F4	Residual fraction	$HClO_4$-HNO_3-HCl-HF (evaporated to near dryness)	–

5000 rpm for 10 min, using a Varian SpectrAA 50B Atomic Absorption Spectrophotometer with air-acetylene flame. The source of radiation was a zinc hollow cathode lamp operating at 5 mA, which provided a 213.9 nm line with a spectral bandwidth of 1.0 nm. The analytical precision was better than 3% relative standard deviation (RSD).

Concentrations of Zn extracted in each sequential extraction step were analysed by ICP-OES at the University of Huelva. The instrument (Jobin Yvon Ultima 2 spectrometer) was calibrated using standard solutions. The analysis was repeated at two different wavelengths to check for any spectral interference. The accuracy and precision of the measurements was better than 3% RSD.

Density functional theory calculations

To obtain quantitative comparison of experimental and theoretical results for geometry optimization density functional theory (DFT), a series of calculations was carried out using the SIESTA code (Soler *et al.*, 2002) within the generalized gradient approximation in the form of Perdew-Burke-Ernzerhof for the exchange-correlation functional (Perdew *et al.*, 1996). The ions were

TABLE 2. Physicochemical parameters, bulk chemical analysis (wt.% oxides) and semi-quantitative mineralogical composition (wt.%) of the soil samples.

Samples	FH-4a	FH-5a	FH-6	Fh-8a	FH-23
Physicochemical parameters					
pH	6.4	6.4	6.9	7.6	7.8
Eh (mV)	438	473	412	390	412
EC (μS/cm)	72.5	96.4	84.7	77.0	58.5
Chemical composition (wt.%)					
SiO_2	53.69	50.34	54.65	42.49	60.42
TiO_2	0.25	0.41	0.85	0.56	0.49
Al_2O_3	6.63	6.88	13.07	11.56	13.73
Fe_2O_3	21.73	18.01	9.10	14.17	9.71
MnO	1.34	1.56	0.59	0.84	0.67
MgO	2.16	2.73	6.51	8.33	2.78
CaO	0.34	0.24	1.58	4.44	0.34
Na_2O	0.07	0.10	0.31	0.23	0.38
K_2O	1.24	2.37	2.43	2.30	2.54
P_2O_5	0.10	0.11	0.13	0.13	0.09
BaO	0.97	2.36	0.34	0.09	0.22
ZnO	0.96	0.68	0.32	1.01	0.32
LOI	9.9	10.8	10.3	13.2	8.3
Total	99.38	96.59	100.18	99.35	99.99
Mineral composition (wt.%)					
Quartz	+++	+++	+++	++	+++
Feldspars	+	+	+	+	++
Illite/muscovite	++	+++	+++	++	+++
Vermiculite	++	++	++	+++	++
Kaolinite	+	+	+	+	+
Talc	–	–	+	+	+
Hematite	+	+	–	+	–
Goethite	+	+	–	+	+
Amphibole	–	–	+	+	–
Dolomite	–	–	–	+	–
Baryte	–	+	–	–	–

+++ (>30%); ++ (10-30%); + (<10%); – not detected

described by norm-conserving atomic pseudopotentials generated using the Troullier-Martins scheme (Troullier & Martins, 1991). Wave functions were expanded in a plane-wave basis set up to an energy cut-off of 300 Ry. The self-consistent field tolerance was set at $1x10^{-5}$ eV/atom. For structural optimization, Brillouin-zone integrations were performed using a $2 \times 1 \times 1$ Monkhorst-Pack grid (Monkhorst & Pack, 1976) giving one k-point which is sufficient due to the large size of the unit cell. The Materials Studio 6.0 software was used to visualize the results (Materials Studio Modeling, 2010).

The simulation lattice was set to periodic boundary conditions in order to reproduce the infinite space. Full variable-cell geometry optimization was conducted for each configuration in order to reduce the external pressure due to the substitution and to characterize the most stable structure. Atoms and water molecules in the structure were allowed to relax to the lowest energy configuration. Due to the compromise between calculation accuracy and computational time for large cells with around 400 atoms and eight different atomic species, the convergence criteria in equilibrium geometries were relaxed freely by the conjugate gradient method until the forces were less than 0.1 eV/Å.

RESULTS AND DISCUSSION

Basic soil characterization

The soil samples were dark brown in colour (dominant hue: 10YR dry) and had a uniformly silty loam texture, with less than 10% of clay-sized particles. They are indicative of soils with near-neutral reaction (pH = 6.4−7.8), very low salinity level (EC = 58−97 μS cm^{-1}), and moderately oxidizing conditions (Eh = 390−473 mV).

Soil minerals identified by XRD in all the bulk samples were quartz, feldspars, vermiculite, dioctahedral mica (illite/muscovite) and kaolinite (Table 2). In addition, some samples contained appreciable amounts of iron oxides (hematite and/or goethite) and a variety of accessory phases such as talc, amphibole, baryte and dolomite, inherited from the parent rocks.

The XRD patterns obtained from an oriented vermiculite-rich sample after Mg-saturation are shown in Fig. 1, revealing a series of sharp 00*l* reflections (14.3, 7.12, 4.77 and 3.57 Å) that have been attributed to basal spacings of vermiculite (Douglas, 1989), based on the following diagnostic criteria: (1) the 7.12/14.3 Å peak intensity ratio is very low (0.25−0.30); (2) upon glycolation no shift was observed in the angular position of the peaks; and (3) heating at 550ºC (even after mild

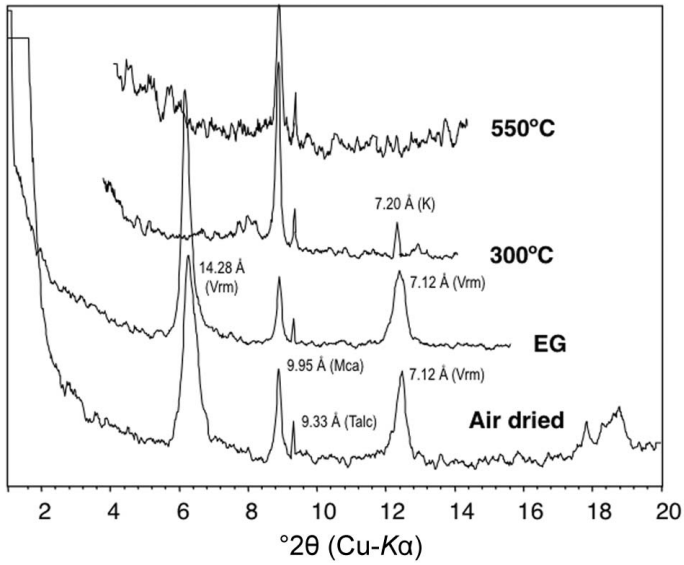

FIG. 1. Typical XRD patterns of oriented aggregates of the soil clays, showing the *d*-spacing after different treatments: untreated (air dried), solvation with ethylene glycol (EG), heated at 300ºC and heated at 550ºC. Mineral abbreviations: Vrm (vermiculite); Mca (mica); K (kaolinite).

heating to 300ºC) caused a contraction of the basal spacing from 14.3 Å to ~10 Å. The effects of these treatments indicate that smectite and chlorite are not present in the samples, at least in any noticeable amount, and that there is no evidence for aluminium hydroxy-interlayered forms of either vermiculite or smectite (Barnhisel & Bertsch, 1989; Meunier, 2007). The 14.3 Å peak showed a narrow full width at half maximum (FWHM = 0.23–0.27º 2θ) suggesting a well-ordered vermiculite mineral (Bortoluzzi *et al.*, 2008).

The chemical composition of major elements is dominated by Si, Al, Fe, Mg and K, clearly reflecting the mineral composition of the soils (Table 2). However the most remarkable result is that all the samples showed elevated Zn contents (0.33–1.01% ZnO), with maximum values (8110 mg kg^{-1}) exceeding by up to two orders of magnitude the regional soil geochemical baseline (Galán *et al.*, 2008), and within the range of values above which ecotoxicity is considered possible (Kabata-Pendias & Pendias, 2001).

Geochemical partitioning of Zn in soil

The concentrations of Zn determined by single extractions with $MgCl_2$ and with NH_4OAc varied in the range 4.2–59.6 mg kg^{-1} and 2.1–27.1 mg kg^{-1} respectively (Table 3), accounting for less than 1.1% of the total Zn content in all the samples. $MgCl_2$ and NH_4OAc are the most widely employed reagents for leaching the exchangeable fraction (Filgueiras *et al.*, 2002). Accordingly, the exchangeable and weakly adsorbed fraction of Zn can be considered to be practically negligible, despite the multiple sorption sites of vermiculite for Zn retention via cation exchange mechanisms.

The amounts of Zn sequentially extracted from the samples studied are shown in Table 3 and their relative portions in the operationally defined fractions are depicted graphically in Fig. 2. The sum of the metal concentrations extracted at each step agreed well with the total digestion results. The recoveries were satisfactory (92–107%).

The results from the sequential extraction procedure showed systematic trends in Zn extractability. More than 80% of the total concentration of Zn present in the soil samples remained in the residual fraction (F4). This suggests that most Zn is tightly bound to the silicate phases of the crystal structure. The proportion of Zn associated with reducible soil components (F2), such as amorphous or crystalline Fe oxy-hydroxides, accounted for up to 10%. The remaining Zn was almost evenly fractionated into the oxidizable (bound to organic ligands) and the acid-soluble/exchangeable fractions. In fact, a minor percentage of Zn (<5%) was bonded to ion-exchange sites of soil particles, in agreement with the findings from the single extractions, except for the sample FH-8a in which the readily extractable Zn accounted for 7.5% due to the occurrence of carbonates (acid-soluble phase).

TABLE 3. Total concentration of Zn in soil samples, and mean concentrations of Zn extracted by single and sequential chemical extractions. All values are expressed in mg kg^{-1}.

Samples	FH-4a	FH-5a	FH-6	FH-8a	FH-23
Total concentration in soil	7680	5540	2640	8110	2630
Single extractions					
1 M $MgCl_2$	26.4±2.3	59.6±5.3	3.3±0.0	17.5±0.1	4.2±0.8
1 M NH_4AcO	11.5±0.5	21.4±1.2	0.6±0.0	27.1±2.2	2.1±0.1
Sequential extraction					
F1 (acid soluble/exchangeable)	195±4.0	295±11	8.2±0.3	623±25	69±4.5
F2 (reducible)	572±23	610±21	21±1.2	334±58	135±8
F3 (oxidizable)	254±30	265±19	10±0.7	30±4.6	49±1.0
F4 (residual)	7032±75	4797±93	2383±21	7305±40	2494±145
Σ (F1+F2+F3+F4)	8053	5967	2422	8292	2747
Recovery (%)	104	107	92	102	104

Vermiculite as an effective sink for Zn

Vermiculite usually occurs in the silt particle-size fraction of the soil, as partly pseudohexagonal plates ranging in size from 10 to 40 μm (Fig. 3). SEM-EDS analysis revealed that Zn is hosted mainly in the crystal lattice of vermiculite. A typical EDS spectrum for these particles (Fig. 3b) shows the presence of Zn in detectable levels, which back-scatters electrons (BSE) strongly; hence vermiculite appears brighter in the BSE images (Fig. 3c). Colour-gradient qualitative elemental mapping obtained by WDS-EPMA showed that most of the Zn and Mg is extensively associated with vermiculite crystals, whereas Al and Fe are present mostly in dioctahedral mica and iron oxides, respectively (Fig. 4).

Quantitative EPMA analysis of vermiculite at particle scale (Table 4) confirmed that ZnO is present in concentrations between 2.05 and 9.11 wt.% ZnO. Three specimens with low (2.26% ZnO), medium (6.02% ZnO) and high Zn contents (9.11% ZnO) were selected for the crystal structure analysis. For each specimen, several computational models were used to evaluate the energy stability by considering three case studies: (1) with all Zn as exchangeable cation in the interlayer space; (2) with all Zn in octahedral sites replacing to some Mg ions; and (3) with varying proportions of Zn in both interlayer space and octahedral sheets.

The theoretical structural model used in our calculations is based on the geometry described by Vahedi-Faridi & Guggenheim (1999). It was supposed that hydrogen atoms were bound to

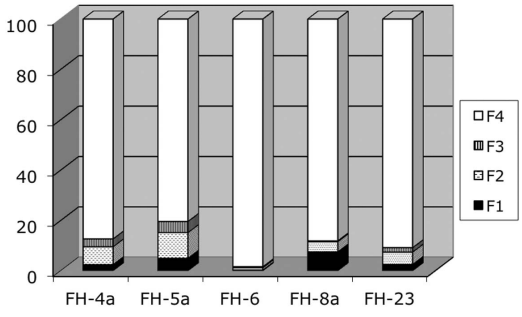

FIG. 2. Geochemical partitioning of Zn (extractable percent) among the fractions operationally-defined from the sequential extraction protocol: F1 (acid soluble/exchangeable); F2 (reducible); F3 (oxidizable); F4 (residual).

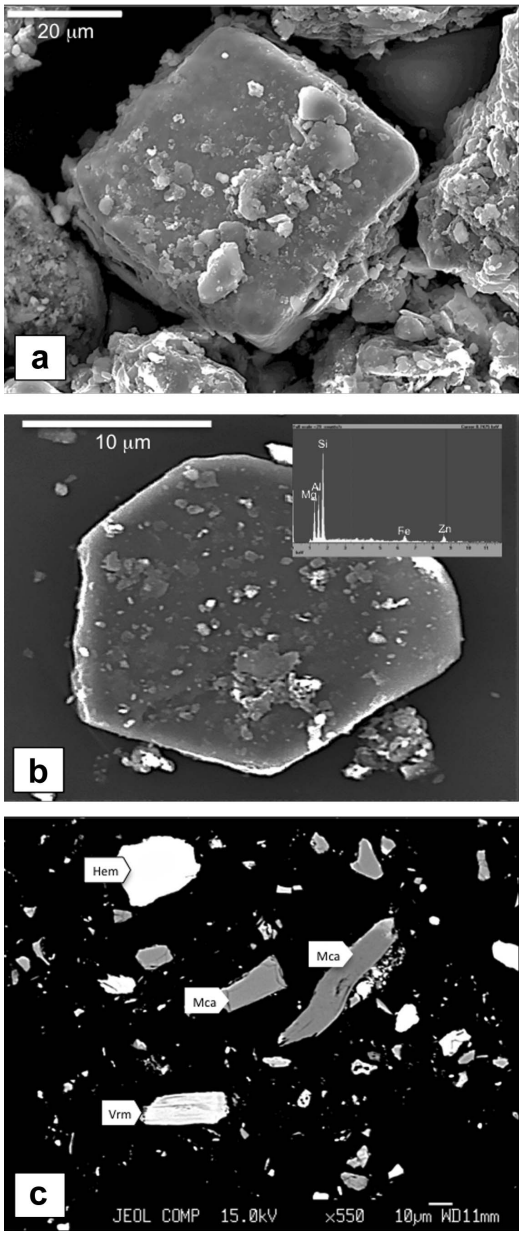

FIG. 3. Secondary electron images showing vermiculite flakes on hematite pseudomorph after pyrite cube (a) and a subeuhedral crystal of vermiculite along with its EDS spectrum (b), and back-scattered electron image (c) showing the contrast between Zn-vermiculite (brighter) and mica. Mineral abbreviations: Vrm (vermiculite); Mca (mica); Hem (hematite).

TABLE 4. Quantitative EPMA analysis (wt.% oxides) of selected vermiculite crystals, and structural formulas on the basis of 10 oxygen atoms and 2 hydroxyls per formula unit.

Analyses	1	2	3	4	5	6	7	8	9	10
SiO_2	35.98	31.89	36.01	33.19	33.64	32.38	32.96	35.19	33.26	35.77
Al_2O_3	21.59	19.95	22.15	20.96	20.15	19.97	23.09	18.68	19.58	22.01
TiO_2	0.32	0.36	0.63	0.58	0.28	0.77	0.50	0.37	0.19	0.27
FeO(t)	2.60	4.30	3.15	2.86	3.67	3.02	4.50	4.06	2.70	4.04
MgO	22.28	20.07	22.68	21.43	20.96	21.77	19.65	22.3	21.13	22.14
MnO	0.12	0.91	0.08	0.12	0.06	0.28	0.13	1.13	0.12	0.12
ZnO	2.26	5.07	2.05	8.37	6.02	6.48	3.57	2.24	9.11	1.61
CaO	0.90	0.62	0.87	0.72	0.38	0.35	0.77	0.81	0.43	0.63
Na_2O	0.07	0.16	0.15	0.14	0.12	0.14	0.11	0.08	0.17	0.04
K_2O	0.08	0.09	0.15	0.03	0.04	0.03	0.13	0.23	0.05	0.04
Total	86.20	83.42	87.92	88.4	85.32	85.19	85.41	85.09	86.74	86.67
Si	2.66	2.58	2.62	2.50	2.59	2.51	2.51	2.69	2.56	2.64
Al	1.34	1.42	1.38	1.50	1.41	1.49	1.49	1.31	1.44	1.36
$\Sigma^{(IV)}$	4	4	4	4	4	4	4	4	4	4
Al	0.54	0.42	0.52	0.36	0.42	0.34	0.59	0.37	0.34	0.55
Ti	0.02	0.02	0.03	0.03	0.02	0.04	0.03	0.02	0.01	0.01
Fe	0.16	0.28	0.19	0.16	0.24	0.20	0.29	0.26	0.17	0.25
Mn	0.01	0.06	0.00	0.01	0.00	0.02	0.02	0.07	0.01	0.01
Zn	0.12	0.29	0.11	0.42	0.34	0.37	0.20	0.13	0.52	0.09
Mg	2.15	1.93	2.15	2.02	1.98	2.03	1.87	2.15	1.95	2.09
$\Sigma^{(VI)}$	3	3	3	3	3	3	3	3	3	3
Mg	0.30	0.41	0.31	0.39	0.43	0.49	0.36	0.39	0.48	0.34
Ca	0.07	0.05	0.07	0.06	0.03	0.06	0.06	0.07	0.06	0.06
Na	0.00	0.01	0.01	0.01	0.01	0.01	0.01	0.01	0.01	0.01
K	0.00	0.00	0.01	0.00	0.00	0.00	0.01	0.00	0.00	0.00
Σ(interlayer)	0.37	0.47	0.40	0.46	0.47	0.56	0.44	0.47	0.55	0.41

oxygen atoms forming hydroxyl groups in octahedral sheets, and these positions were optimized. Moreover, two layers of water in the interlayer space were considered in this study for two reasons: first, this hydration state often occurs in vermiculites under natural conditions in soils (Zhou *et al.*, 1993); and second, this configuration implies a thickness of the structural unit in line with the XRD-measured basal spacing (~14.3 Å).

The composition of vermiculite was calculated on the basis of 10 oxygen atoms and 2 hydroxyls per formula unit (half unit cell content), and assuming all iron to be ferrous. Structural formulae (Table 4) show that Si varies between 2.50 and 2.69 apfu (atoms per formula unit) and the octahedral sheets contain mostly Mg (from 1.87 to 2.19 apfu), consistent with a high-charge trioctahedral vermiculite. The Zn content ranges from 0.09 to 0.52 apfu. The layer charge deficiency (0.7−1.0 per formula unit) is balanced by hydrated exchangeable cations in the interlayer space, notably Mg and very minor amounts of Ca and Na.

The structural formulae of the three vermiculite crystals selected to perform the theoretical analysis were as follows:

$$[Mg_{0.30},Ca_{0.07},Zn_{0.12-x}][Mg_{2.15},Al_{0.54},Fe_{0.16},Zn_x][Si_{2.66},Al_{1.34}]O_{10}(OH)_2{\cdot}nH_2O$$

$$[Mg_{0.43},Ca_{0.03},Zn_{0.34-x}][Mg_{1.98},Al_{0.42},Fe_{0.24},Zn_x][Si_{2.59},Al_{1.41}]O_{10}(OH)_2{\cdot}nH_2O$$

$$[Mg_{0.48},Ca_{0.06},Zn_{0.52-x}][Mg_{1.95},Al_{0.34},Fe_{0.17},Zn_x][Si_{2.56},Al_{1.44}]O_{10}(OH)_2{\cdot}nH_2O$$

where: x may range from 0 to total Zn content in each specimen; $x = 0$ for models with all Zn atoms in the interlayer space; x = total Zn content for models with all Zn atoms in octahedral sites, and $0 < x <$ total Zn content for intermediate cases.

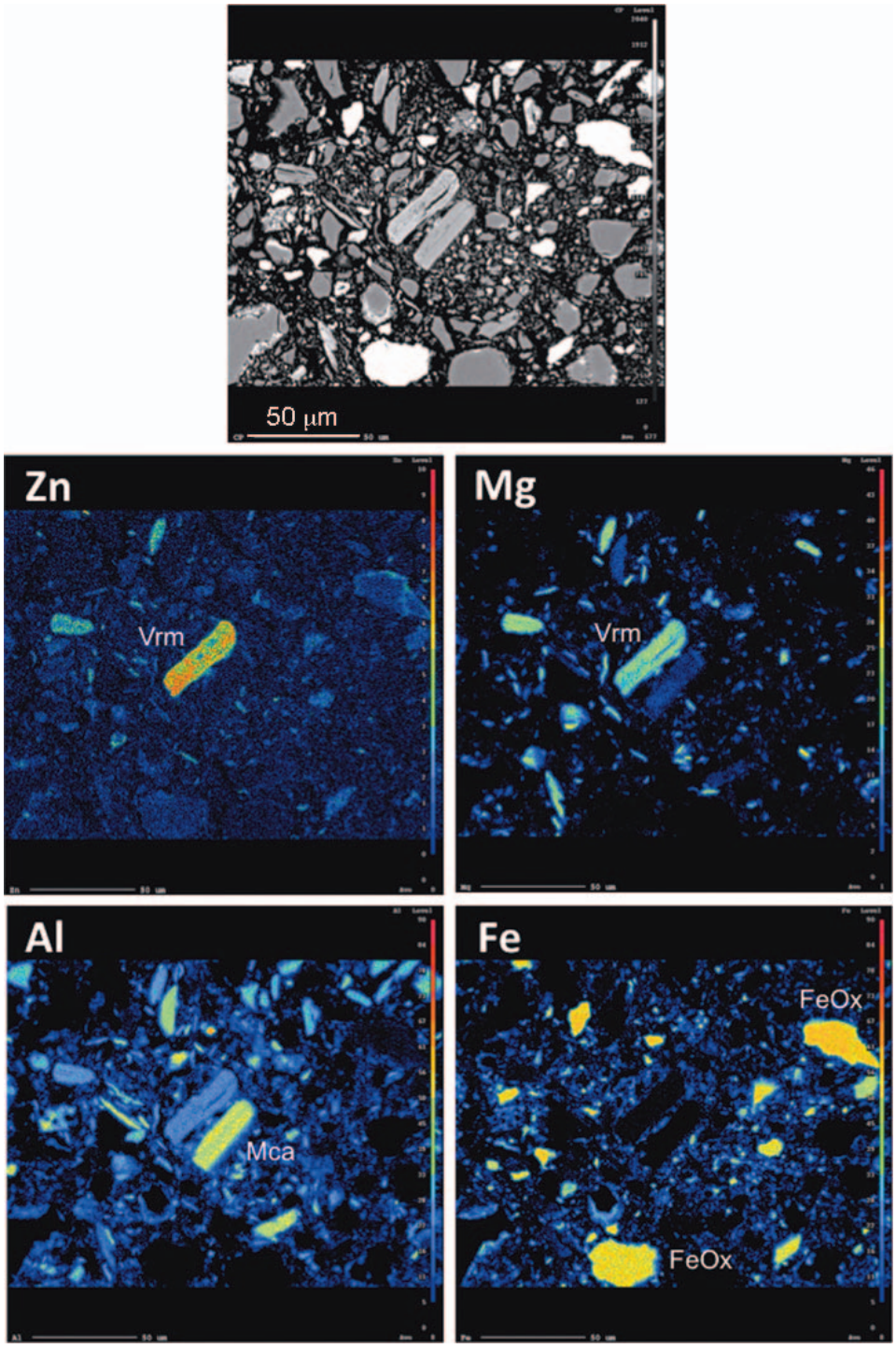

FIG. 4. Qualitative elemental mapping images showing the spatial distribution of Zn, Mg, Al and Fe in soil minerals. Mineral abbreviations: Vrm (vermiculite); Mca (mica); FeOx (iron oxides). The scale bars are 50 μm long.

TABLE 5. Crystal cell parameters for the models of vermiculite with one (model $_1V_{Zn}$), three (model $_3V_{Zn}$) and five (model $_5V_{Zn}$) atoms of Zn. Values obtained by other authors are shown for comparison.

Model*	– Rates (%) – Zn-oct	Zn-int	*a* (Å)**	*b* (Å)**	*c* (Å)**	— Angles (º) — α, γ	β	Volume (Å^3)	Energy (eV)	ΔE (eV)***
$_1V_{Zn}{}^{1oct}$	100	0	26.89	9.35	15.03	90.4,90.3	96.4	3755.65	−88474.7261	
$_1V_{Zn}{}^{1int}$	0	100	26.94	9.34	15.04	90.3,90.3	96.4	3760.1	−88474.5064	0.22
$_3V_{Zn}{}^{3oct}$	100	0	27.08	9.35	14.92	90.90.3	96.6	3756.65	−91343.4858	
$_3V_{Zn}{}^{2oct\text{-}1int}$	67	33	27.1	9.34	14.94	90.2,90.3	96.5	3761.04	−91343.1650	0.32
$_3V_{Zn}{}^{1oct\text{-}2int}$	33	67	27.1	9.35	14.93	89.9,90.4	96.6	3759.26	−91342.9044	0.58
$_3V_{Zn}{}^{3int}$	0	100	27.1	9.35	14.93	90.90.4	96.6	3760.84	−91342.7211	0.76
$_5V_{Zn}{}^{5oct}$	100	0	27.04	9.32	14.88	90.4,90.2	96.5	3726.44	−94302.2738	
$_5V_{Zn}{}^{4oct\text{-}1int}$	80	20	27.04	9.31	14.87	90.2,90.2	96.5	3714.94	−94302.1254	0.15
$_5V_{Zn}{}^{3oct\text{-}2int}$	60	40	27.03	9.31	14.88	90.2,90.2	96.5	3718.33	−94301.8376	0.44
$_5V_{Zn}{}^{2oct\text{-}3int}$	40	60	27.04	9.3	14.87	90.3,90.3	96.5	3720.47	−94301.7830	0.49
$_5V_{Zn}{}^{1oct\text{-}4int}$	20	80	27.04	9.3	14.87	90.2,90.3	96.6	3717.75	−94301.7179	0.56
$_5V_{Zn}{}^{5int}$	0	100	27.03	9.3	14.87	90.2,90.3	96.5	3715.3	−94301.5799	0.69
Gruner (1934)			5.3	9.2	14.29−14.39	90.0	97.15	–	–	
Mathieson & Walker (1954)			5.33	9.18	14.45	90.0	97	701.76	–	
Walker (1955)			~5.32	~9.25	14.36−14.81	90.0	97−101	~690	–	

* Models $V_{Zn}{}^{int}$ = 100% of interlayer Zn; models $V_{Zn}{}^{oct}$ = 100% of octahedral Zn; model $V_{Zn}{}^{(X)oct\text{-}(1-x)int}$ with $0 < x <$ total Zn number for intermediate configurations.

** The parameter *a* of the unit cell of our models of vermiculite is increased by a factor of five.

*** Respect to the model with all Zn atoms in the octahedral sites.

Given that Mg occupies both structural positions, i.e. exchangeable and octahedral, computational simulations were started by first optimizing the structure (atomic positions and lattice parameters) for pure Mg-vermiculite with two layers of interlayer water molecules. The interlayer cations are solvated in outer-sphere complexes with the water molecules. Full details of the Mg-water exchangeable complexes for a double layer of water in the interlayer can be found in Shirozu & Bailey (1966). Then, isomorphous substitutions of Mg by other cations (Fe, Al and Zn) were promoted in the two possible structural sites of our unit cell model. According to the structural formulae, a single unit cell contains non integer numbers of cations. For computing stable structures of periodic lattices, the edge *a* of the unit cell was increased by a factor of five. Thus, a $5 \times 1 \times 1$ supercell was used, in which atoms were rounded off to the nearest integer number. The resulting chemical formulae contain one (model ${}_1V_{Zn}$), three (model ${}_3V_{Zn}$) and five (model ${}_5V_{Zn}$) atoms of Zn:

$${}_1V_{Zn} = [Mg_3,Ca_1,Zn_{1-x}][Mg_{21},Al_5,Fe_2,Zn_x][Si_{27},Al_{13}]O_{100}(OH)_{20}\cdot 60H_2O$$

$${}_3V_{Zn} = [Mg_4,Zn_{3-x}][Mg_{20},Al_4,Fe_2,Zn_x][Si_{26},Al_{14}]O_{100}(OH)_{20}\cdot 60H_2O$$

$${}_5V_{Zn} = [Mg_5,Ca_1,Zn_{5-x}][Mg_{20},Al_3,Fe_2,Zn_x][Si_{25},Al_{15}]O_{100}(OH)_{20}\cdot 60H_2O$$

The results obtained for the geometry optimization and substitution of Zn in the interlayer space and in octahedral sheets are listed in Table 5. According to the theoretical calculations, the presence of Zn inside the vermiculite structure does not significantly change the cell parameters in comparison with those observed in earlier studies (e.g. Mathieson & Walker, 1954; Walker, 1955). The results obtained in the computational simulations (Table 5) are in agreement with measurements of basal spacing by XRD. In turn, these data confirm the existence of two layers of water in the interlayer domain.

Regarding the energetic stability, DFT calculations showed that the more stable structure corresponds to the models with all Zn occupying the octahedral sites. Thus, the isomorphous substitution of Mg by 100% of Zn in six-fold coordination is more stable by 0.22 eV, 0.76 eV and 0.69 eV than 100% of Zn in the interlayer spaces for the models ${}_1V_{Zn}$, ${}_3V_{Zn}$ and ${}_5V_{Zn}$, respectively (Table 5). These small deviations in energy are enough to explain isomorphous substitutions of similar cations in phyllosilicates that do not undergo notable unit cell size changes (Sáinz-Díaz *et al.*, 2002; Timón *et al.*, 2004).

In vermiculite models with Zn cations occupying simultaneously both structural positions, it was also observed that higher Zn percentage in octahedral sites induces greater structural stability. Hence, it seems that Zn cations are preferentially located at the octahedral positions of vermiculite, which would drastically reduce their mobility in soils under ambient conditions. It is worth noting that the relationship between energy stability and octahedral Zn percentage in the model ${}_5V_{Zn}$ is not linear. As clearly observed, the more stable configurations with 80% and 100% of octahedral Zn are separated from the remaining models by a relatively higher energy gap than the differences observed between specimens. Consequently, a slight substitution of Zn in the interlayer could be also be favourable energetically. These findings are in good agreement with the metal partitioning model obtained by sequential chemical extraction.

CONCLUSIONS

Experimental and theoretical results from this work have implications for long-term retention of Zn in soil. Metal released by weathering of carbonate-hosted sulfide mineralization was immobilized and unevenly partitioned among the various pedogenic phases, allowing for the accumulation of high levels of Zn in the chestnut grove soils, which become a hot spot of environmental concern. Selective chemical extractions showed that most of the Zn remained in the residual fraction, tightly bound to the silicate matrix of the samples, whereas in the soil exchangeable Zn pool, which potentially is the most harmful for the environment, it was practically negligible. Therefore, it may be concluded that most of the Zn occurs in an irreversible non-exchangeable form associated with lattice entrapment, and therefore is unavailable for plant uptake. Results from XRD, SEM-EDS and EPMA analyses provided evidence that pedogenic vermiculite was the most notable Zn scavenger. Our computational simulation supports the conclusion that Zn is structurally bound in vermiculite and resides in octahedral sites rather than in interlayer exchange positions, as predicted by DFT calculations.

Sequestration of Zn in the octahedral sheets of vermiculite led to long-term natural attenuation of significant inputs of geogenic Zn.

ACKNOWLEDGMENTS

We thank the UGRGrid (University of Granada) for permitting the use of their computational resources.

REFERENCES

Arribas A., Bechstädt T. & Boni M. (1990) Stratabound ore deposits related to synsedimentary tectonics: South-West Sardinia (Italy) and Sierra de Aracena (Spain); a comparison. *Geologische Rundschau*, **79**, 373–386.

Barnhisel R.I. & Bertsch P.M. (1989) Chlorites and hydroxy-interlayered vermiculite and smectite. Pp. 729–788 in: *Minerals in Soil Environments* (J.B. Dixon & S.B. Weed, editors). Soil Science Society of America, Madison, Wisconsin, USA.

Biscaye P.E. (1965) Mineralogy and sedimentation of recent deep-sea clay in the Atlantic Ocean and adjacent seas and oceans. *Geological Society of America Bulletin*, **76**, 803–832.

Bortoluzzi E.C., Velde B., Pernes M., Dur J.C. & Tessier D. (2008) Vermiculite, with hydroxy-aluminium interlayer, and kaolinite formation in a subtropical sandy soil from south Brazil. *Clay Minerals*, **43**, 183–195.

Douglas L.A. (1989) Vermiculites. Pp. 635–674 in: *Minerals in Soil Environments* (J.B. Dixon & S.B. Weed, editors). Soil Science Society of America, Madison, Wisconsin, USA.

Evans L.J. (1989) Chemistry of metal retention in soils. *Environmental Science & Technology*, **23**, 1046–1056.

Fernández-Caliani J.C., Requena A., Sáez R. & Ruiz de Almodóvar G. (1989) Las mineralizaciones de Pb-Zn asociadas a rocas carbonatadas en el sector de Fuenteheridos (Huelva). *Studia Geologica Salmanticensia*, **4**, 7–15.

Filgueiras A.V., Lavilla I. & Bendicho C. (2002) Chemical sequential extraction for metal partitioning in environmental solid samples. *Journal of Environmental Monitoring*, **4**, 823–857.

Galán E., Fernández-Caliani J.C., González I., Aparicio P. & Romero A. (2008) Influence of geological setting on geochemical baselines of trace elements in soils. Application to soils of Southwest Spain. *Journal of Geochemical Exploration*, **98**, 89–106.

Gruner J.W. (1934) The structures of vermiculites and their collapse by dehydration. *American Mineralogist*, **19**, 557–575.

Jacquat O. (2008) *Long-term fate of zinc in contaminated soils: Zinc speciation by synchrotron spectroscopy and chemical extractions.* PhD Thesis, Swiss Federal Institute of Technology, Zurich, 152 pp.

Jacquat O., Voegelin A., Villard A., Marcus M.A. & Kretzschmar R. (2008) Formation of Zn-rich phyllosilicate, Zn-layered double hydroxide and hydrozincite in contaminated calcareous soils. *Geochimica et Cosmochimica Acta*, **72**, 5037–5054.

Jacquat O., Voegelin A., Juillot F. & Kretzschmar R. (2009a) Changes in Zn speciation during soil formation from Zn-rich limestones. *Geochimica et Cosmochimica Acta*, **73**, 5554–5571.

Jacquat O., Voegelin A. & Kretzschmar R. (2009b) Local coordination of Zn in hydroxy-interlayered minerals and implications for Zn retention in soils. *Geochimica et Cosmochimica Acta*, **73**, 348–363.

Jacquat O., Voegelin A. & Kretzschmar R. (2009c) Soil properties controlling Zn speciation and fractionation in contaminated soils. *Geochimica et Cosmochimica Acta*, **73**, 5256–5272.

Juillot F., Morin G., Ildefonse P., Trainor T.P., Benedetti M., Galoisy L., Calas G. & Brown G.E. Jr. (2003) Occurrence of Zn/Al hydrotalcite in smelter-impacted soils from northern France: Evidence from EXAFS spectroscopy and chemical extractions. *American Mineralogist*, **88**, 509–526.

Junta de Andalucía (1989) *Mapa de Suelos de Andalucía a escala 1:400.000.* http://www.juntadeandalucia.es/medioambiente.

Kabata-Pendias A. & H. Pendias (2001) *Trace Elements in Soils and Plants*. 3rd edition. CRC Press, Boca Raton, Florida, USA.

Manceau A., Lanson B., Schlegel M.L., Hargé J.C., Musso M., Eybert-Bérard L., Hazemann J.L., Chateigner D., & Lamble G.M. (2000) Quantitative Zn speciation in smelter-contaminated soils by EXAFS spectroscopy. *American Journal of Science*, **300**, 289–343.

Manceau A., Marcus M.A., Tamura N., Proux O., Geoffroy N., & Lanson B. (2004) Natural speciation of Zn at the micrometer scale in a clayey soil using X-ray fluorescence, absorption, and diffraction. *Geochimica et Cosmochimica Acta*, **68**, 2467–2483.

Materials Studio Modeling (2010) Accelrys Software Inc., San Diego, California, USA.

Mathieson A.M. & Walker G.F. (1954) Crystal structure of magnesium vermiculite. *American Mineralogist*, **39**, 231–255.

Meunier A. (2007) Soil hydroxy-interlayered minerals: A re-interpretation of their crystallochemical properties. *Clays and Clay Minerals*, **55**, 380–388.

Monkhorst H.J. & Pack J.D. (1976) Special points for Brillouin-zone integrations. *Physical Review B*, **13**, 5188.

Perdew J.P., Burke K. & Ernzerhof M. (1996) Generalized gradient approximation made simple. Physical Review Letters, 77, 3865–3868.

Pérez-Cid B., Lavilla I. & Bendicho C. (1998) Speeding up of a three-stage sequential extraction method for metal speciation using focused ultrasound. Analytica Chimica Acta, **360**, 35–41.

Quevauviller P., Rauret G., Muntau H., Ure A.M., Rubio R., López-Sánchez J.F., Fiedler H.D. & Griepink B. (1994) Evaluation of a sequential extraction procedure for the determination of extractable trace metal contents in sediments. *Fresenius Journal of Analytical Chemistry*, **349**, 808–814.

Rich C.I. (1968) Hydroxy interlayers in expansible layer silicates. *Clays and Clay Minerals*, **16**, 15–30.

Sáinz-Díaz C.I., Timón V., Botella V., Artacho E. & Hernández-Laguna A. (2002) Quantum mechanical calculations of dioctahedral 2:1 phyllosilicates: Effect of octahedral cation distributions in pyrophyllite, illite, and smectite. *American Mineralogist*, **87**, 958–965.

Scheinost A.C., Kretzschmar R., Pfister S. & Roberts D.R. (2002) Combining selective sequential extractions, X-ray absorption spectroscopy, and principal component analysis for quantitative zinc speciation in soil. *Environmental Science & Technology*, **36**, 5021–5028.

Schultz L.G. (1964) *Quantitative interpretation of mineralogical composition from X-ray and chemical data for the Pierre Shale*. United States Geological Survey, Professional Paper, 391-C.

Shirozu H. & Bailey S.W. (1966) Crystal structure of a two-layer Mg-vermiculite. *American Mineralogist*, **51**, 1124–1143.

Soler J.M., Artacho E., Gale J.D., García A., Junquera J., Ordejón P. & Sánchez-Portal D. (2002) The SIESTA method for ab initio order-N materials simulation. *Journal of Physics: Condensed Matter*, **14**, 2745–2779.

Timón V., Sáinz-Díaz C.I., & Hernandez-Laguna A. (2004) Hydrogen bonding and vibrational properties of hydroxyl groups in the crystal lattice of dioctahedral clay minerals by means of First Principles calculations. *Physics and Chemistry of Minerals*, **31**, 475–486.

Troullier N. & Martins J.L. (1991) Efficient pseudopotentials for plane-wave calculations. *Physical Review B*, **43**, 1993–2006.

Ure A.M. (1996) Single extraction schemes for soil analysis and related applications. *Science of the Total Environment*, **178**, 3–10.

Vahedi-Faridi A. & Guggenheim S. (1999) Structural study of mono-methylammonium and dimethylammonium-exchanged vermiculites. *Clays and Clay Minerals*, **47**, 338–347.

Voegelin A., Jacquat O., Pfister S., Barmettler K., Scheinost A.C. & Kretzschmar R. (2011) Time-dependent changes of zinc speciation in four soils contaminated with zincite or sphalerite. *Environmental Science & Technology*, **45**, 255–261.

Walker G.F. (1955) The mechanism of dehydration of Mg-vermiculite. *Clays and Clay Minerals*, **4**, 101–115.

Yin K., Hong H., Churchman G.J., Li R., Li Z., Wang C. & Han W. (2013) Hydroxy-interlayered vermiculite genesis in Jiujiang late Pleistocene red earth sediments and significance to climate. *Applied Clay Science*, **74**, 20–27.

Zhou P., Amarasekera J., Solin A., Mahanti S.D. & Pinnavaia T.J. (1993) Magnetic properties of vermiculite intercalation compounds. *Physical Review B*, **47**, 486–493.